7474 *Macromolecules* **2009**, *42*, 7474–7484
DOI: 10.1021/ma901131c

Macromolecules
ARTICLE

Onset of Entanglements Revisited. Topological Analysis

C. Tzoumanekas,*,†,‡ F. Lahmar,§ B. Rousseau,§ and D. N. Theodorou†,‡

†*National Technical University of Athens, School of Chemical Engineering, Zografou Campus, GR-15780 Athens, Greece,* ‡*Dutch Polymer Institute (DPI), P.O. Box 902, 5600 AX Eindhoven, The Netherlands, and* §*Laboratoire de Chimie Physique, Université Paris-Sud 11, UMR 8000 CNRS, Orsay, France*

Received May 25, 2009; Revised Manuscript Received August 12, 2009

ABSTRACT: In a series of two papers, we study the onset of entanglements and the transition from Rouse-type to reptation dynamics, in the context of dissipative particle dynamics (DPD) simulations of a coarse-grained polymer melt. A set of monodisperse systems with increasing chain length is examined. We consider both static and dynamic aspects of the problem. Part I, this paper, deals with the continuous change of the polymer topology, from unentangled (short chains), to entangled (long chains). We show that as chain length increases the rate of increase of chain overlap increases asymptotically. It becomes constant when chains are sufficiently long, and in this regime a long chain topology is established. Next, we examine the onset by probing static length scales at the level of primitive paths (PPs). A simple scaling model based on a transformation of PPs from thin rods (short chains) to random walks (RWs) (long chains) is discussed qualitatively and quantitatively. The model predicts a crossover in the underlying topology, which leads to a Rouse to reptation transition in dynamics when PP conformations change from rods to to RWs. The entanglement molecular weight is interpreted as the crossover length of this transition. The predicted M_c/M_e ratio is one, which, though small, is compatible with packing length independence and the suppression of contour length fluctuations within the model. Part II, the following paper (DOI 10.1021/ma9011329), deals with dynamic aspects of the onset of entanglements, making possible a comparison between static and dynamic length scales.

1. Introduction

It is well-known that above the glass-transition temperature (T_g) any flexible polymer, as chain length increases, transforms from a short chain unentangled liquid to a long chain entangled melt, which can support stress. Dynamics and rheology of the system also change from Rouse type to reptation type.[1,2] At the molecular level, this dynamical and rheological 'transition' is due to a gradual increase of chain overlap which leads to chain entanglement.

In a series of two papers, we study the transition from a Rouse-like behavior to the reptation regime. The present paper, from now on called part I, is dedicated to the static, structural and topological analysis of the entanglement network, with a particular emphasis on the transition region. The following paper, from now on called part II,[3] examines the transition from a dynamical point of view, using both a local and global dynamical analysis. Using these two approaches, it is possible to compare the evolution of static measures of topology with corresponding dynamic length scales, as chain length increases. As far as we know, such a comparison has not been presented previously in the literature.

Generation and relaxation of entangled polymer models, at a molecular level, gives rise to excessively high demands in simulation time, due to the long relaxation times induced by entanglements.[4] In order to reduce the computational effort, coarse-grained models, in which several atoms are represented by a single particle,[5,6] may be used. Although coarse-grained models leave out many chemical details of the real system, structural and dynamical aspects can still be examined. The system studied here is a coarse grained polyethylene-like (PE) model based on the work[7] by Guerrault et al., with some force-field enhancements (see part II[3]). The level of coarse-graining is such that excluded volume interactions are softened[5,8] and chain crossing is possible. In order to prevent chain crossing and recover an entangled behavior in the limit of long chains, a specific segmental repulsion potential has been included. The coarse-graining procedure and the strategy followed in order to maintain chain uncrossability are presented in detail in part II.[3] The dynamics is generated using the dissipative particle dynamics (DPD) method. This type of stochastic dynamics, with pairwise conservative, dissipative (friction) and random forces, takes full advantage of the soft nature of the particles. From DPD simulations, we extract local dynamical length scales by using Rouse mode analysis, and global dynamical length scales by examining the self-diffusion coefficient, the end-to-end distance relaxation time, the shear relaxation modulus and the viscosity. Since the uncrossability constraint introduced in our model is responsible for the dynamical transition, we believe that our results and conclusions are fairly general.

Part I is concerned with the topological analysis (TA) of configurations generated along the DPD trajectories. TA[9−13] is able to provide the static length scales of a network of topological constraints (TCs) underlying the melt system. The network is generated by coarse graining polymer chains to the level of primitive paths (PPs). The latter are constructed using the CReTA algorithm[11] which reduces chain conformations to corresponding shortest paths in a way envisaged by Doi and Edwards.[2] A typical length scale, the chain length between entanglements or, equivalently, the entanglement mass M_e, can be extracted from the PPs.

PPs are promising intermediates in the multiscale modeling of both linear and branched polymer chains in the entangled state.[13−18] Thus, it is very interesting to look into the onset of entanglements at the PP level. As we discuss in the paper, in such an approach we have to treat the tube diameter and M_e as varying length scales which have to be defined for short chain systems too. Their usual meaning is recovered in the long chain limit.

Initially, we will show that as chain length, N, increases, chain overlap increases at an N-dependent rate which is different from

*To whom correspondence should be addressed. E-mail: tzoumanekas@gmail.com.

 Published on Web 09/10/2009

Table 1. Number of Beads per Chain, N, Number of Chains, N_{ch}, Time Step, δt, End-to-End Vector Decorrelation Time, τ, and Number of Frames, N_{fr}, in the DPD Trajectories of the Systems Studied

N	N_{ch}	δt (ns)	τ (ns)	N_{fr}
6	100	0.01	0.59	1200
8	100	0.02	1.09	1000
10	100	0.04	2.15	1000
12	100	0.06	3.16	1000
15	90	0.1	5.81	1000
20	80	0.2	11.9	1000
30	80	0.5	44.2	1200
40	80	1.0	87.8	800

the constant rate in the asymptotic long chain regime (large N). The rate is controlled by the N-dependence of the contour length density (or mass density ρ), and of the stiffness of the system (or characteristic ratio C_N), both of which increase with N until they reach chain length independent values.

The increasing chain overlap leads to gradual changes in the underlying system topology. At the level of PPs, these changes can be described by a continuous structural transition of PP conformations. The latter, as chain length increases, transform from thin rods to random walks (RWs). The transition signifies the onset of a long chain topology, characteristic of the system. It takes place in a crossover N-regime between the rod regime, where the PP length $L_{pp}(N)$ scales as $L_{pp} \propto (C_N N)^{1/2}$, and the RW regime where $L_{pp} \propto N$. Within our approach, the crossover chain length corresponds to the entanglement length N_e.

We then present a simple scaling model based on an early work of Doi.[19] The model connects the crossover regime in dynamics and rheology with the crossover regime in the variation of PP length, $L_{pp}(N)$. It leads to a continuous transition from Rouse-type to strict-reptation dynamics, as a result of the rod to RW transition of PP conformations. In part II,[3] the model is compared with simulation results on the diffusion coefficient, the relaxation time of the end-to-end vector, and the viscosity.

2. Systems Studied

Eight systems of coarse-grained PE with the number of beads per chain, N, varying from 6 to 40 as shown in Table 1, were generated by the DPD method. Each bead represents the center of mass of a $C_{20}H_{40}$ unit. Part II[3] describes in detail the bottom-up approach utilized for deriving interaction potentials. To prohibit chain crossing due to the softness of interactions in DPD, an additional segmental repulsion potential (SRP) was introduced between segments of different chains. The set of parameters chosen for the SRP was such that binary chain encounters lead to 2×10^{-4} crossing events per time step (on the average), and a dynamical behavior consistent with reptation theory (see part II[3]).

The DPD simulations were performed in the canonical ensemble (NVT), at a temperature of 450 K, and at the density of long chain PE, $\rho = 0.761$ g/cm^3. For each system a long enough dynamical trajectory, which allows for dynamical renewal of the underlying topology, has been analyzed. Simulation details relevant to the topological analysis are presented in Table 1. The reader should refer to part II[3] for other system details.

3. Results

3.1. Stiffness, Contour Length Density and Packing Length. Table 2 summarizes some structural features of each system studied. We focus on quantities which are relevant to the entanglement problem.

The ratio of the mean squared end-to-end distance, R^2, to the mean squared radius of gyration, R_g^2, is practically 6, which is the expected value for ideal chains in a polymer melt. The characteristic ratio is denoted as C_n, when calculated by

Table 2. Structural Features of Systems Studied[a]

N	C_N	C_n	R^2/R_g^2	ν (nm^{-2})	p (Å)	f
6	1.63	4.28	5.77	1.67	3.02	0.94
8	1.68	4.60	5.87	1.75	2.81	1.01
10	1.73	4.84	5.94	1.79	2.66	1.07
12	1.76	4.99	5.97	1.83	2.58	1.12
15	1.77	5.11	5.99	1.86	2.52	1.18
20	1.82	5.31	6.00	1.89	2.42	1.26
30	1.83	5.43	5.99	1.92	2.36	1.36
40	1.79	5.36	5.95	1.94	2.39	1.43

[a] See text for an explanation.

mapping chain dimensions to the original atomistic PE systems, and as C_N for the coarse systems, i.e.

$$C_N = \frac{R^2}{(N-1)l_{cg}^2}, \quad C_n = \frac{R^2}{nl^2} \tag{1}$$

where $n = 20N-1$ is the number of chemical bonds corresponding to an atomistic PE chain, $l = 1.54$ Å is the average PE skeletal bond length, and $l_{cg} = 12.1$ Å is the root mean squared bond length in the coarse systems (approximately equal to the average bond length). Both ratios increase with chain length and approach an asymptotic value, a behavior characteristic[20] of polymer melts. The asymptotic value of C_n (see Table 2) is smaller[21] than the characteristic ratio of PE, $C_\infty^{PE} \sim 8$, at $T = 450$ K, due to the SRP which 'squeezes' chain dimensions (because it was introduced after parametrizing the coarse grained PE potential, see part II[3]). For the coarse systems the largest part of chain rigidity is hidden in the beads (blobs), and thus C_N is much smaller than C_n. The simplest dependence of C_N on chain length[20] is of the form $C_N = C_\infty + A/(N-1)$, where C_∞ is the asymptotic long chain value, and A is a constant. A corresponding fit is shown in Figure 1a. Best fit values are $C_\infty = 1.85$, and $A = -1.12$.

In Table 2 and in Figure 1b we also present the contour length density,

$$\nu = \frac{N_{ch}L}{V} = \frac{1}{w^2} \tag{2}$$

where N_{ch} is the number of chains, and L is the average chain contour length. The inverse of ν corresponds to an average chain cross-sectional area w^2 (assuming homogeneous melt density), and thus w corresponds to the average distance between chain contours. As chains become longer, ν increases and approaches an asymptotic value. For very long chains ν is proportional to the bead density, which for our systems is constant. The chain length dependence of ν is an artificial chain-end effect of the coarse-graining procedure, which will be discussed in the next section. For this reason, and for all purposes of this study, the contour length density should be conceived as the mass density of the system.

The packing length, p, has gained attention[22-25] as a structural parameter capturing the influence of structure on melt rheology. It is defined as $p = V_{ch}/R^2$, where V_{ch} is the average volume per chain. Experimentally, it has been found[22] that a scaling of the form $M_e \propto \rho p^3$ shows a good correlation with a very large number of entangled polymers. The packing length can also be defined as

$$p = \frac{w^2}{b} = \frac{1}{\nu b} \tag{3}$$

where it is expressed as a combination of the two independent length scales, which according to Graessley and

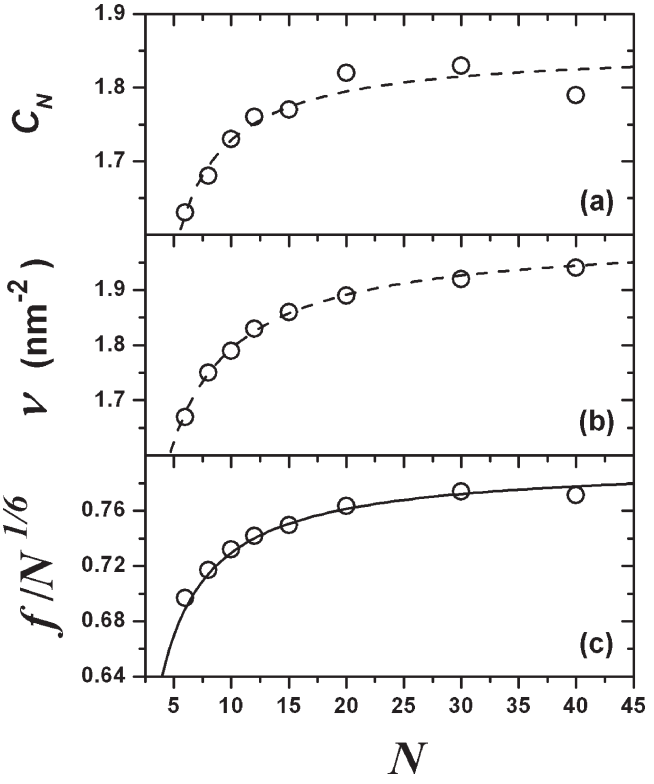

Figure 1. Characteristic ratio C_N (a), contour length density ν (b), and reduced degree of overlap (c) of systems studied. The dashed lines are fits to the data. The solid line is an analytic expression based on the fits in parts a and b. See text for an explanation.

Edwards[26,27] rule the entanglement problem: the average distance w between chain contours (controlled by density), and the Kuhn length, b, which is a measure of stiffness and is proportional to C_N.[25]

It is interesting to examine what is the effect of the variation of these length scales on p as chain length increases. From Table 2, we see that the packing length gradually decreases with increasing N before reaching a limiting long chain value, the one that is related with M_e. This decay is expected to be characteristic of all polymer melts, since, in general, both the stiffness and the mass density increase before becoming N-independent, in the transition from a short to long chain system. Our system follows this general behavior, and is thus suitable for studies related with the onset of entanglement effects.

3.2. Chain End Concentration and Coarse Graining Effects. Although all systems are prepared at a constant ρ (or bead number density), ν is not constant, but increases as chain length increases. This effect is exaggerated here due to the application of the blob picture[5,7,28] as a simulation scheme, by utilizing the NVT ensemble. In this procedure, since the beads (blobs) are point-like particles located at the center of mass of a backbone sequence, a certain "length" from the ends of the atomistic chain cannot be represented at the coarse level.[29] On the other hand, by preparing the coarse systems at the density of PE, the volume is adjusted to the full contour length of the atomistic systems. Since as N increases chain end concentration decreases, then, at the coarse level, the "missing" length from chain ends leads to a gradual increase of ν with N. Finally, for long chain systems, where the chain end concentration vanishes, ν approaches an asymptotic value. The effect becomes smaller if a shorter sequence is associated with a bead, and it is a source of underestimation of C_n. This underestimation, however, becomes negligible for very long chains.

Interestingly, a gradual increase of ν with chain length is the behavior expected of a real polymer melt.[21] There, however, ρ and ν increase in the same manner until they reach an asymptotic long chain value, characteristic of the material. For example, as shown in Figure 1b, a hyperbolic fit of the form

$$\nu = \frac{\nu_\infty}{1 + \alpha/N} \tag{4}$$

which can accurately fit density[21] data in real polymers, provides a good fit to the ν data. ν_∞ denotes the contour length density at infinite N, while α is a dimensionless constant describing the rate at which ν increases with N. The best fit values are $\nu_\infty = 2.00\ \mathrm{nm}^{-2}$, and $\alpha = 1.15$. In real polymers, the hyperbolic dependence is due to the excess exluded volume[30] associated with chain ends in comparison to interior segments, which, for short chain systems leads to a smaller density. Here, while the density is constant, the same N-dependence can describe ν data because the increase of ν with N is again a chain-end effect, but for different reasons.

A decreasing chain end concentration, besides affecting the density of the system, plays a crucial role in entanglement formation. For example, Kavassalis and Noolandi[31,32] have emphasized how chain "tail" concentration affects the onset of entanglements, in a context which leads to the packing length concept.[25] We conclude this section by pointing out that the displayed N-dependence of ν is a desirable feature of studies related with the onset of entanglements and, though introduced artificially in our simulations, is qualitatively correct.

3.3. Chain Overlap. As chain length increases, chains start to penetrate the pervaded volume of each other, a process which eventually leads to formation of entanglements and complex rheological behavior. A measure of the degree of chain overlap is the ratio of the mean chain size, to the mean distance between centers of mass of chains, $\ell = V_{\mathrm{ch}}^{1/3}$,

$$f = \frac{R_g}{\ell} = \left(\frac{R_g}{6p}\right)^{1/3} \tag{5}$$

which can also be expressed through the packing length. Another measure of overlap, which is often used in the literature, is the ratio n_g of the total contour length in the pervaded volume of a chain, to the average chain contour length in the same volume, L. A definition or calculation of the average pervaded volume is difficult,[28] and in general it is considered[22] to be proportional to ${R_g}^3$, with a prefactor of order one. Such an estimation suffices for qualitative arguments. Thus, n_g can be written as

$$n_g \propto \frac{\nu {R_g}^3}{L} = \left(\frac{{R_g}^3}{V_{\mathrm{ch}}}\right) = \frac{R_g}{6p} = f^3 \tag{6}$$

and, as we see, is proportional to the third power of f. Note that n_g can also be viewed as the average number of chains in the pervaded volume of a chain.[28] Within this view, n_g counts the number of whole chains sharing the pervaded volume. In reality, small parts of many chains are within each chain's pervaded volume, and n_g counts these parts as if they were connected into chains of N beads.[28]

Ideally, chain interpenetration starts at $f \simeq 1$ and increases continuously with N. However, overlap initiation does not necessarily mean the onset of entanglements, which is expected for a sufficient degree of overlap. Additionally, both

R_g, ℓ, and therefore their ratio, follow some distribution. Thus, microscopically, interpenetration will not start at exactly $f = 1$. Also, it will not be uniform (present for all chains and to the same degree) when entanglement starts, and before chains become sufficiently long. Moreover, for a dense polymer melt, f cannot take values much smaller than one, as it can in a solution. Actually, even for very short, unentangled chain systems, it is expected that $f \simeq 1$.

By inspecting Table 2, we see that our systems start from a regime where $f \simeq 1$. Then, as N increases, the degree of chain overlap increases with a rate determined by N-dependence of R_g and p, i.e., by the N -dependence of C_N and ν. When the latter approach their asymptotic values, beyond, $N \gtrsim 20$, f increases like $f \propto N^{1/6}$, a scaling law expected for long chain systems. In Figure 1, where we plot $f/N^{1/6}$, the developing plateau illustrates this behavior. A similar plateau is observed for $n_g/N^{1/2}$ (not presented). The solid line in Figure 1c is a plot of a corresponding analytic form for $f/N^{1/6}$, based on the approximate analytic expressions of C_N and ν used in the fits of Figure 1a, Figure 1b. The parameters C_∞, A, ν_∞, and α, used in the plot were presented in previous sections.

The features of increasing stiffness and density, which gradually attain an N-independent value, are normally encountered in all flexible polymer melts. As chain length increases, these features give rise to a crossover in the way chains interpenetrate each other. Initially, chain overlap develops with an N-rate controlled by the variation of C_N and ν. In this regime, the rate of increase of chain overlap is chemistry dependent. Then, chain overlap proceeds with a universal rate, $f \propto N^{1/6}$.

3.4. Topological Analysis. DPD trajectories were subjected to topological analysis by using the CReTA[11] algorithm. For each N, we have analyzed half of the frames of Table 1, which were chosen to be equally spaced in time. All averages in this section are over these frames.

CReTA is a geometric coarse-graining algorithm, which reduces a dense system of polymer chains to the corresponding system of primitive paths (PPs). The latter are constructed as shortest paths,[2] which are under the same 'topological constraints' (TCs) as the original chains. Operationally, chain ends are fixed in space, and by prohibiting chain crossing, the contour lengths of all chains are simultaneously minimized (shrunk), until they become sets of rectilinear strands coming together at the nodal points of a network. The nodal points are the TCs generated by chain uncrossability.[11]

In the case of a system where all chains are free of TCs, CReTA *reduces them to straight lines* (*rods*). As the algorithm proceeds, in order to facilitate contour reduction through the removal of unentangled loops, chain thickness is progressively reduced toward a zero value. The final thickness used for acquiring the results below was 0.6 Å. Explanatory videos of the whole process can be found in the Supporting Information of ref 11, and in ref 33. For other details, similar approaches, and a comparison between them see refs 9−12, 34, and 35.

On the basis of the tube model, the tube diameter, d, and the entanglement molecular weight, N_e (measured in number of beads here), correspond to the length and the mass of the Kuhn segment of the primitive path. They characterize the smallest length scale where PPs are viewed as entropic strands.[2] We estimate these quantities from

$$d = \frac{R^2}{L_{pp}}, \quad N_e = N\frac{R^2}{{L_{pp}}^2} \tag{7}$$

where L_{pp} is the average PP contour length. d and N_e reflect a length scale defined by the underlying system topology.

Table 3. Topological Measures of Systems Studied[a]

N	d (Å)	$N_e(N)$	n_t	δ (Å)	d/R	P_{ch}	N_{TC}	N^*_{TC}
6	34.02	5.75	11.22	4.22	0.98	0.67	3.00	1.82
8	38.10	6.70	13.53	4.93	0.91	0.82	3.14	2.20
10	41.33	7.48	15.52	5.37	0.86	0.89	3.30	2.56
12	43.30	7.95	16.79	5.64	0.81	0.94	3.37	2.75
15	45.42	8.55	18.04	5.96	0.75	0.97	3.52	3.07
20	48.17	9.24	19.89	6.25	0.68	0.99	3.65	3.38
30	50.27	9.82	21.29	6.54	0.57	1.00	3.76	3.66
40	50.37	9.99	21.08	6.71	0.50	1.00	3.85	3.81

[a] See text for an explanation.

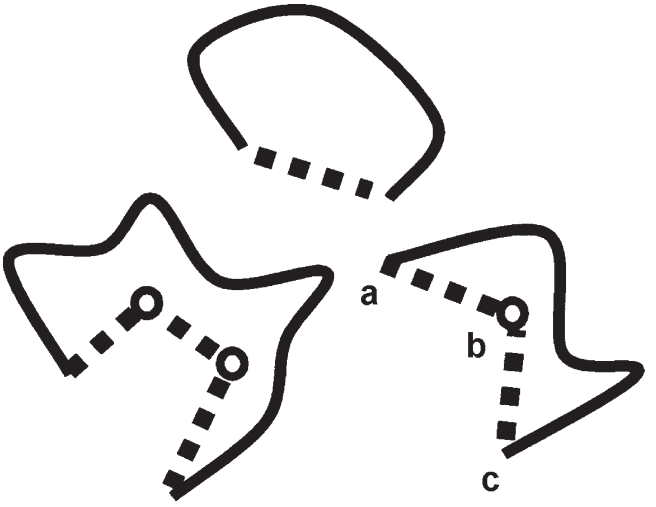

Figure 2. Schematic representation of short chain PPs (dashed lines) in 2D. After contour shrinking of all chains, with chain ends fixed, two of the chains are *constrained*, i.e., restricted by shortest paths of other chains (not shown), with local conformations perpendicular to the plane. The circles denote binary TCs. The PP of the *unconstrained* chain is a straight line (a thin rod). The length difference of solid and dashed lines, divided by N, is the chain slack per bead δ. Note that PP end strands, like ab, bc, contribute to both averages, N_{TC}, N^*_{TC}, (see text).

From the above relations, they can be defined for unentangled systems too, as long as L_{pp} can be defined for short chain systems. This issue will be discussed in the next section. The above equations correspond to the "Graessley/Fetters" definition of N_e, as it has been discussed in ref 36. ${L_{pp}}^2/R^2$ corresponds to the number of Kuhn (tube) segments of the PP.

In the following sections we will also use the symbol $\widetilde{N}_e$ in order to express a PP Kuhn segment as a number of bonds of the coarse-grained chain. Since,

$$\widetilde{N}_e = (N-1)\frac{R^2}{{L_{pp}}^2} = \left(1-\frac{1}{N}\right)N_e \tag{8}$$

numerically, $\widetilde{N}_e \to N_e$ when $N \to \infty$, though in different units.

In Table 3, we summarize some results from our analysis. $\delta = (L - L_{pp})/N$, denotes the average amount of chain slack per bead, which is consumed by the contour reduction operation applied by CReTA (see Figure 2). n_t is the number of entanglement strands (PP Kuhn segments) in a cubed tube diameter,

$$n_t = d^3\frac{N_{ch}}{V}\frac{N}{N_e} = \frac{d}{p} \tag{9}$$

which is expressed very simply through the packing length. Lin[37] proposed this number as a fundamental aspect of topological universality in polymer viscoelasticity. For flexible polymers it has a universal value $n_t = 20.6 \pm 8\%$.[25] Our

estimation for the long chain systems ($N = 30, 40$) is $n_t \sim 21$. The extremely good agreement with the universal number is a coincidence.

N_e can be estimated from the long chain systems. We find that $N_e \simeq 10$ beads, corresponding to 200 methylene units. In order to compare with PE, we can use the scaling relation $M_e \propto \rho p^3$. We have to take into account that the density of our systems is that of PE, and that the estimated characteristic ratios C_n are smaller than C_∞^{PE} of real (atomistic) PE (due to the SRP, see section 2). By scaling p of the $N = 40$ system through a stiffness factor C_n/C_∞^{PE}, we get a scaled packing length $p' = pC_n/8 = 1.60$ Å, which is very close to 1.65 Å, a value characteristic[22] of PE. Additionally, by scaling our N_e estimation through a factor $(p'/p)^3$ we get a corresponding PE value of $N_e \simeq 60$ methyl units. The latter is in good agreement with experimental estimates ($N_e = 61.4$) based on plateau modulus measurements,[22] and with values obtained[11] by a similar methodology applied to atomistic PE ($N_e = 74.2$).

3.5. Topological Constraints. Within CReTA, TCs are resolved to specific beads along PP contours, at places where shortest paths restrict each other from further contour reduction.[11] For each chain, a series of strands connecting chain ends and TCs forms the corresponding PP. Here, in order to avoid confusion with the established sense of entanglement, chains with their corresponding shortest path being a straight line (just one strand connecting chain ends) are characterized as *unconstrained*. On the other hand, chains which are subject to TCs have shortest paths which are not straight lines.[11] These are characterized as (topologically) *constrained* (see Figure 2). We avoid to characterize *constrained* chains as "entangled", since, as we will show in next sections and in part II,[3] TCs exist (microscopically) even for systems which are dynamically unentangled.

In short chain systems a part of the system consists of unconstrained chains, while the rest of the system (constrained chains), generates a percolated network (at the level of PPs). Percolation in a system of thin rods (unconstrained chains) can be driven by a small concentration of TCs. However, the appearance of TCs (in a system of unconstrained chains) as chain length increases, is not related with a state where PPs differ substantially from thin rod-like objects. In this regime, on the average, the network part of the PP system is generated by mildly deformed rods. Moreover, TCs cannot promote reptation and can be considered as short-lived interchain contacts. As it will become clear in next sections and in part II,[3] it is our static approach, based on chain shrinking and shortest paths, which in this regime "freezes" interchain contacts in a form of a network of TCs.

Regarding the number of chains involved in a TC, here, we consider all TCs as binary (like a slip-link which constrains two chains). In reality, we find that in long chain systems $\sim 3\%-5\%$ are ternary (a link constrains three chains). The length scale defined by TCs is the average length between successive TCs along a chain. This is also the average length of a network edge. In Table 3 we provide two estimations of this length scale, both measured in number of beads. N_C^* is an average which takes into account only constrained chains, while N_{TC} is an average over all chains (see Figure 2). *Unconstrained* chains contribute to N_{TC} as strands with N beads. Note that in ref 11, N_{TC} is denoted as N_{ES}. In the case of a system where all chains are unconstrained, $N_{TC} = N$, and $N_C^* = 0$. For a fully constrained system, $N_{TC} = N_C^*$, while $N_{TC} \neq N_C^*$ for systems with both constrained and unconstrained chains. By comparing N_C^* with N_{TC} we can follow the development of uniformity and integrity of the underlying network, as chain length increases (see next section).

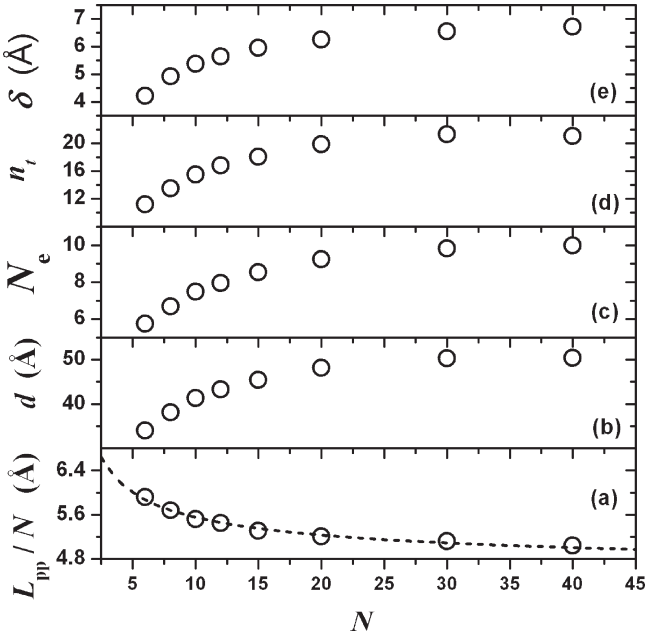

Figure 3. Estimations of the PP length per bead L_{pp}/N (a), tube diameter d (b), the entanglement length N_e (c), the number of entanglement segments per cubed tube diameter n_t (d), and the chain slack per bead δ (e) from topological analysis. The dashed line is a guide for the eye.

The fraction of "constrained" chains is denoted by P_{ch}. The length scale defined by N_{TC} is shorter than N_e. Orientational correlations[11] between successive steps of the PP (of average length N_{TC}), make the PP Kuhn segment larger than the step-length of the PP. For this reason, an entanglement in the sense defined by the tube model is associated with more than one successive TCs along a chain.[11,12] This is similar to the relation between the Kuhn segment and the bond length of a real chain.

3.6. Onset of a Long Chain Topology. In this section. we discuss, from a topological and static point of view, the transition from *unconstrained* to fully *constrained* chains (in the sense defined in the previous section), as chain length increases. In Figure 3 we present, d, N_e, n_t, and δ, as functions of N. All quantities increase monotonically and approach chain length independent values. For d and N_e, this feature has been observed in all previous studies based on the reduction of polymer chains to PPs.[12,38−41] From eq 7, we see that the gradual increase of these topological measures is controlled by the N-dependence of R^2, L_{pp}. The variation of L_{pp}/N with N is shown in Figure 3a. It decays and approaches a chain length independent value. An analytic form for L_{pp} with similar behavior was recently deduced[18] within a slip-link model context.

The observed trends boil down to the N-dependence of C_N and ν, presented in Figure 1. As N increases, the stiffness increases and the mean spacing between chain contours, $w = \nu^{-1/2}$, decreases. These quantities determine how chains are packed and intertwined in 3D space, and thus the amount of chain slack per bead, δ. The latter becomes independent of chain length (see Figure 3), when C_N and ν finally approach their asymptotic values. From then on, the underlying topology is fixed (in the statistical sense[11]). This behavior is clearly seen in Figure 3, though the asymptotic regime extends in longer chain lengths, as will become clear in next section.

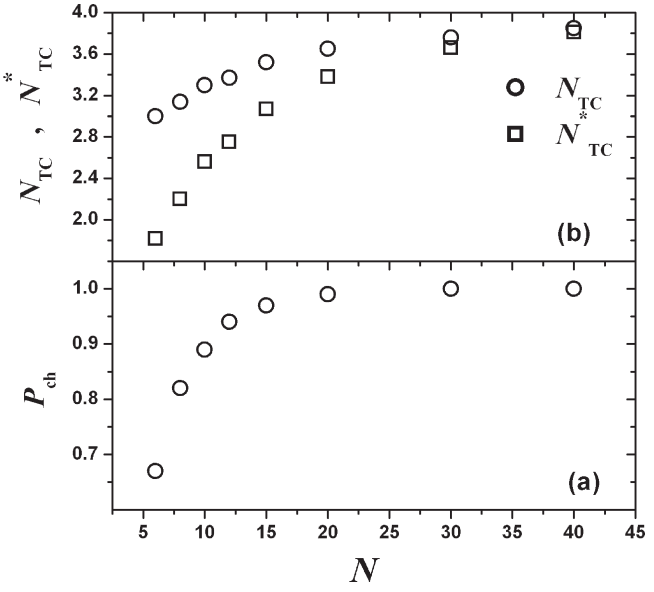

Figure 4. Estimations of the proportion of chains which are *constrained* P_{ch} (a), and of the length scale defined by TCs N_{TC}, N^*_{TC} (b). See text for an explanation. We note that in ref 11, N_{TC} is denoted as N_{ES}.

Qualitatively, the variation of L_{pp} with N can be understood as follows. In short chain systems, chains are free of TCs and CReTA reduces them to approximately straight lines (rods), i.e., $L_{pp} \cong R \propto (C_N N)^{1/2}$. Thus, L_{pp} is proportional[19] to the end-to-end distance, and therefore, eq 7 leads to $d \simeq R$, $N_e \simeq N$. Within this view, PPs for unconstrained chains are considered as thin rods which connect chain ends. In long chain systems, the presence of a constant density of TCs makes $L_{pp} \propto N$, and therefore, from eq 7, d and N_e become independent of chain length. In between, the density of TCs changes, resulting in the N dependence of L_{pp}, and therefore of d and N_e, which are topological measures reflecting these changes. Note that, conceptually, N_e cannot be defined for unentangled systems. Here, it is treated as a length scale defined by eq 7. This issue is analyzed in the next section.

We note that in our data chain overlap f is still small for the system with $N = 6$, where also $N_e \simeq N$, i.e., $L_{pp} \sim R$. However, systems with very short chains of $N < 6$ would be needed in order to observe the full $L_{pp} \propto (C_N N)^{1/2}$ dependence for unentangled chains.

In Figure 4, we present P_{ch}, N_{TC}, and N^*_{TC}, which can shed some light on the way chains interpenetrate at a microscopic level. P_{ch} for short chain systems is quite large (see Table 3). The proportion of constrained chains starts from 67% for $N = 6$ and grows to 100% as N increases. Tube model theories suggest that a short chain system would be free of TCs, since by increasing chain length initially the system will not follow reptation dynamics. Microscopically, however, a degree of chain interpenetration definitely exists.

From Table 2 we see that for these systems, $f \simeq 1$. Chain length N is at the regime where chains just start to overlap. This is verified from the fact that for $N = 6$, $d/R \simeq 1$, and $N_e \simeq N$, which means that shortest paths are not very far from displaying rod-like conformations. At the same time, the chain slack per bead δ is much smaller than for long chain systems, and less "shrinking" of chains is needed to reveal the TCs. We expect that in this regime TCs are also dynamically different from those in long chain systems. For unentangled systems, some chains could experience the effect of overlap as short-lived TCs, which act as interchain contour contacts. More evidence about this conjecture will appear in part II.[3] We will show that kinetic constraints revealed by Rouse-mode analysis of unentangled systems act at approximately the same length scales as the TCs revealed here.

The picture we envisage is that, as N increases, TCs appear initially at some parts (chains) of the system, and at $N \gtrsim 20$, where $N_{TC} \simeq N^*_{TC}$, the system approaches asymptotically a topologically 'homogeneous and invariant' regime. Homogeneous, in the sense that almost all chains are *constrained* ($N_{TC} \simeq N^*_{TC}$), and invariant, in the sense that topological measures do not change significantly with increasing N. The onset of this topology is achieved when C_N and ν approach N-independent values. Under the same conditions, chain overlap is led to a scaling of the form $f \propto N^{1/6}$, which is expected for long chain systems. In the latter, reptation will probably be promoted by TCs which become long-lived.

A paradox suggested by our results is that N_e is a length scale which increases when p decreases, from the short to the long chain systems. The scaling $M_e \propto \rho p^3$ implies the opposite. However, this scaling is associated with M_e variations due to different chemistry of fully entangled systems. It cannot relate the packing length of short chain systems to M_e, and is extracted from plateau modulus measurements of systems far away from the N-regime where the onset of entanglements takes place. A model for the onset which leads to an N_e that starts from a large value, greater than the chain length, which then decays to an asymptotic value as N increases, is that of Kavassalis and Noolandi.[31,32] In this model the onset is related with a diminishing chain end concentration. Our approach is closer to the work of Doi,[19] where the onset is associated with the change of scaling of the primitive path from $L_{pp} \propto N^{1/2}$, to $L_{pp} \propto N$ (see next sections). Chain end concentration is implicitly taken into account by the N-variation of L_{pp}. The paradox (discussed in the Appendix) boils down to the fact that chain slack is smaller for short chain systems under TCs.

Interestingly, even in the absence of TCs, when all PPs are rods (fully unconstrained system, phantom chains), the chain slack per bond is still smaller for a short chain system. For example, for a freely jointed chain of N_{fj} segments and step length b_{fj},

$$\delta = \frac{L-R}{N_{fj}} = b_{fj}\left(1-\frac{1}{\sqrt{N_{fj}}}\right) \tag{10}$$

Small N_{fj} leads to small δ, because $R/L \propto N_{fj}^{-1/2}$. As $N_{fj} \to \infty$, the end-to-end distance becomes negligible compared to the contour length, and $\delta \to b_{fj}$, an unphysically large value. In the presence of TCs, however, PPs become random walks, and then δ levels off to a value smaller than b_{fj},

$$\delta = \frac{L-L_{pp}}{N_{fj}} = b_{fj}\left(1-\frac{1}{\sqrt{N_e}}\right) \tag{11}$$

which is determined by N_e. In the last equation, N_e is expressed in units of freely jointed segments.

3.7. From Rods to Random Walks. PPs here are defined as shortest paths. The latter do not have any intrinsic stiffness, like real chains. Their conformational characteristics are defined by the underlying system topology. In the absence of microscopic TCs, the shrinking procedure leads to shortest paths which resemble thin 'rod-like' objects. In a highly entangled melt, uncrossability constraints lead to zigzag shaped shortest paths with random walk (RW) statistics.[11] This regime is reached asymptotically by PPs, in a manner similar to the way real

chains acquire random walk conformations with increasing chain length.[20]

The above limiting behaviors and length scales are captured very well by relations 7. In these equations, N_e defines the smallest length scale where chains can be described as entropic strands, due to the presence of conformational restrictions brought about by TCs. The system enters asymptotically a regime where it can support entropic elasticity when $N_e(N) < N$. For rods, $L_{pp} \simeq R$, and since R^2/N is proportional to C_N, when real chains follow RW statistics, $L_{pp} \propto (C_N N)^{1/2}$. In this case conformations are solely restricted by chain ends, and $N_e(N) = N$. Chains are described as (independent) entropic strands at the level of the whole chain.

In the limit of long chains, shortest paths become random walks, with a fixed average step length, when $R \propto N^{1/2}$, and $L_{pp} \propto N$. Then, eq 7 leads to $N_e(N) \rightarrow N_e(\infty) < N$. Between these limiting behaviors, the PP Kuhn segment increases asymptotically and alters the N dependence of $L_{pp}(N)$. For real chains, this effect is captured by the N-dependence of the characteristic ratio. For shortest paths, it is displayed by $d(N)$ in Figure 3. In this intermediate chain length regime, PPs generate an underlying interpenetrating network, but PP conformations have not yet reached the asymptotic regime where they become N-independent.

We also note that, by construction, PPs are described by a smaller number of Kuhn segments than the corresponding real chains. Thus, the asymptotic regime of PPs (constant d) is shifted to longer chain lengths than the asymptotic regime of real chains (chain length where $C_N \simeq C_\infty$). This shift is expected to be chemistry dependent. Thus, while in the melt real chains may be of sufficient length so that the system is in the asymptotic regime, the coarse grained system of PPs could be in a state where PPs are not yet in their corresponding asymptotic regime.

An approximate view on the crossover regime of L_{pp} is attempted below. In order to estimate the asymptotic behavior of L_{pp}, in Figure 5a we plot chain slack reduced by the number of bonds per chain $x = N - 1$; i.e., $\delta = (L - L_{pp})/x$. Since for $N = 6$ we found $d/R \simeq 1$, for $N < 6$ our system is in the "rod-like" regime. Therefore, we enlarge our data set by adding data for $N = 3,4,5$, shown with open squares, where the PP length is approximated as $L_{pp} = R = [xC_N(x)]^{1/2} l_{cg} C_N(x)$ is calculated by using the fit presented in Figure 1a. The data have been fitted by equation,

$$\delta = \delta_\infty - \frac{\beta}{\sqrt{x}} - \frac{\gamma}{x} \tag{12}$$

where δ_∞, β, and γ are fitting constants. The fit, with $\delta_\infty = 7.46$ Å, is shown with a solid line in Figure 5a. Since $L = x l_{cg}$, the corresponding expression for L_{pp} is

$$L_{pp} = \gamma + \beta\sqrt{x} + (l_{cg} - \delta_\infty)x \tag{13}$$

where the second and third term match the rod and RW regime, correspondingly. In principle, $L_{pp}(x)$ could probably be expressed as a function of $C_N(x)$ and $\nu(x)$, but we were not able to identify it. An analytic expression for $L_{pp}(x)$ in the context of slip-link models was given recently in ref 18, and for Gaussian chains by Doi.[19]

A log−log plot of the reduced L_{pp} quantity $L_{pp}/(x[C_N(x)]^{1/2})$ is presented in Figure 5b. This quantity eliminates the $C_N(x)$ dependence of $L_{pp}(x)$, especially in the rod regime, so that the crossover from rods to random walks can be estimated from the intersection of the asymptotes shown in the plot. The open squares are the added data in the rod regime, and the dashed line is a linear fit to these data, with a slope of −0.5

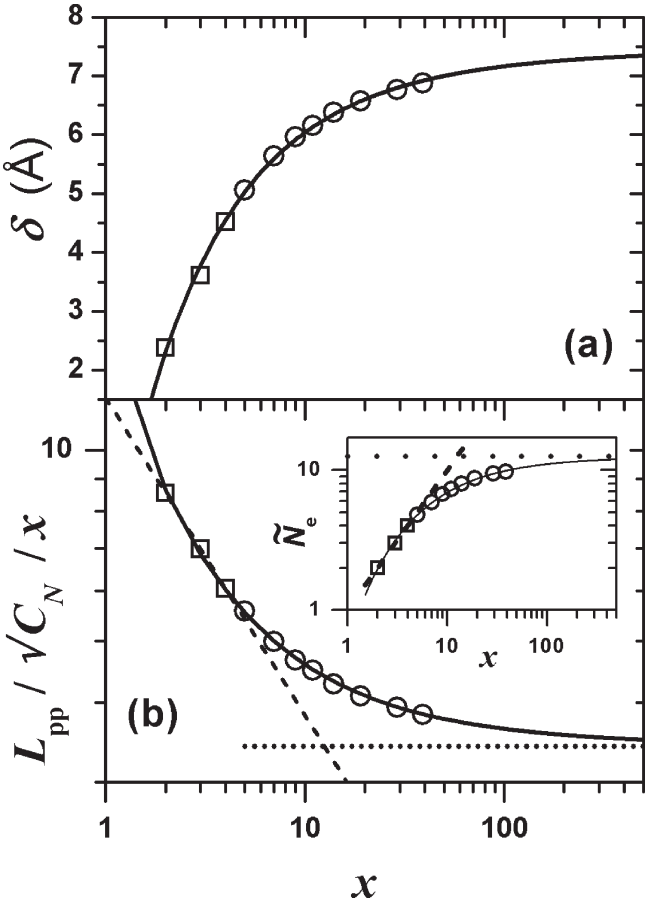

Figure 5. Semilog plot of chain slack per bond δ, (a), and log−log plot of reduced PP length $L_{pp}/(x\sqrt{C_N})$ (b). Squares denote additional data for the "rod regime" of PPs. The solid lines are fits of eqs 12 and 13. The dashed line shows the asymptote for the rod regime of PPs, (with a slope of −0.5), and the dotted line shows the asymptote at $x \rightarrow \infty$, (zero slope). The inset shows $\widetilde{N}_e$ of eqs 8 and 15. The lines in the inset have similar meaning as in part b. The corresponding slopes of the asymptotes are one, and zero. See text for an explanation.

(by construction). The solid line was generated by using the expression for $L_{pp}(x)$ and the fit function for $C_N(x)$. At very short chain lengths the curve deviates from the asymptote due to the approximate form of $L_{pp}(x)$. The dotted line denotes the asymptote at $x \rightarrow \infty$, where

$$\frac{L_{pp}(x)}{x\sqrt{C_N(x)}} \rightarrow \frac{l_{cg} - \delta_\infty}{\sqrt{C_\infty}} \tag{14}$$

The inset in Figure 5b presents the same crossover as it appears when plotting $\widetilde{N}_e(x)$. The solid line denotes

$$\widetilde{N}_e(x) = l_{cg}{}^2 \frac{x^2 C_N(x)}{L_{pp}{}^2(x)} \tag{15}$$

and the dashed line denotes the line $\widetilde{N}_e(x) = x$, which corresponds to $N_e(N) = N$. The dotted line is the asymptote at $x \rightarrow \infty$, where $\widetilde{N}_e(x) \rightarrow N_e(N)$, so that the intersection is at

$$N_e(\infty) \rightarrow \frac{l_{cg}{}^2 C_\infty}{(l_{cg} - \delta_\infty)^2} \simeq 12.6 \tag{16}$$

In both plots of Figure 5b, the intersection is located (by construction) at the same crossover value $N_e(\infty) \simeq 12.6$. In the scheme we have described above, as chain

length increases the underlying topology leads to a gradual transformation of shortest path conformations from rods to RWs. Within this scheme, the entanglement molecular weight, $N_e(\infty)$, is interpreted as the crossover chain length. Our basic assumption is that for $N < 6$ the PP conformations are rod-like, and that in this regime $L_{pp} = R$. It is also evident that our systems fall into the crossover regime of the underlying topology. Figure 5 shows that the asymptotic regime is reached at much longer chain lengths.

We note that, throughout the analysis we have assumed that in the rod regime $\langle L_{pp}\rangle = \langle R\rangle \simeq R$, where R is the root-mean square of the end-to-end distance. For Gaussian chains, $\langle R\rangle = (8/3\pi)^{1/2}R \simeq 0.92R$. For simplicity, this issue was not considered in our analysis, though, short chains are not necessarily Gaussian.

3.8. Dynamics and Rheology. In the context of Gaussian chains and reptation dynamics, Doi has shown[19] that by increasing the concentration of fixed obstacles in the reptation model, the N dependence of the mean PP length changes continuously from $L_{pp} \propto N^{1/2}$, for low concentration, to $L_{pp} \propto N$, for large concentration. At the same time, the chain self-diffusion constant, D_{CM}, and the relaxation time of the end-to-end vector, τ, were shown to scale as

$$D_{CM} \propto {L_{pp}}^{-2}, \quad \tau \propto N(L_{pp})^2 \tag{17}$$

Thus, chain dynamics change continuously from Rouse-type where

$$D_{CM} \propto N^{-1}, \quad \tau \propto N^2 \tag{18}$$

to de Gennes-type where

$$D_{CM} \propto N^{-2}, \quad \tau \propto N^3 \tag{19}$$

as the concentration of obstacles increases, and this change is ascribed to a continuous change of the N-dependence of L_{pp}.

In our case, in the rod regime $L_{pp} \propto (C_N(x)x)^{1/2}$, and in the RW regime $L_{pp} \propto x$, where x is the number of bonds. In the rod regime $L_{pp} = R$, and thus L_{pp} is independent of contour length density. In order to map the rod to RW transition of PP conformations, to the Rouse to reptation crossover in dynamics, we have to eliminate from $L_{pp}(x)$ the stiffness dependence in the rod regime, and thus we work with $L_{pp}/(C_N(x))^{1/2}$. In the same manner, the crossover in the previous section was determined by plotting $L_{pp}(x)/([C_N(x)]^{1/2}x)$ The contour length density (or chain end concentration) dependence of $L_{pp}(x)$ is buried in eq 13. In the RW regime there is no dependence of $L_{pp}(x)$ on $C_N(x)$ or the density, since both become constant for large x.

Thus, within our scheme, the corresponding scaling expressions based on Doi's work are

$$D_{CM} \propto \left(\frac{L_{pp}(x)}{\sqrt{C_N(x)}}\right)^{-2}, \quad \tau \propto x\left(\frac{L_{pp}(x)}{\sqrt{C_N(x)}}\right)^{2} \tag{20}$$

In order to get a corresponding expression for the viscosity, we work as follows. In general, $\eta \propto G(\tau)\tau$, where $G(\tau)$ is the relaxation modulus and τ is the relaxation time of the end-to-end vector. For the plateau modulus G we have

$$G \propto \frac{\rho N_A k_B T}{M_e} \propto \frac{1}{N_e(N)} \tag{21}$$

Within our model, in the rod regime $N_e(N) = N$ and $\tau \propto N^2$. This leads to Rouse-type scalings for G and η,

$$G \propto \frac{1}{N}, \quad \eta \propto N \tag{22}$$

In the RW regime of PPs, since the modulus is constant ($N_e(N)$ is constant), and $\tau \propto N^3$, we find the reptation-type scaling, $\eta \propto N^3$. Thus, since

$$N_e \propto \frac{xR^2(x)}{{L_{pp}}^2(x)} \propto \frac{x^2 C_N(x)}{{L_{pp}}^2(x)} \tag{23}$$

the x, $L_{pp}(x)$, $C_N(x)$ dependence of G, can be written as

$$G \propto \frac{1}{N_e(x)} \propto \frac{1}{x^2}\left(\frac{L_{pp}(x)}{\sqrt{C_N(x)}}\right)^2 \tag{24}$$

and then we have for η

$$\eta \propto G\tau \propto \frac{1}{x}\left(\frac{L_{pp}(x)}{\sqrt{C_N(x)}}\right)^4 \tag{25}$$

The above relation leads to $\eta \propto x$ in the rod regime, and $\eta \propto x^3$, in the RW regime of PPs. The dynamical crossover given by relations 20 and 25 will be compared against dynamical data of D_{CM}, τ, η, in part II.[3]

In the scaling scheme above and in the Doi−Edwards theory,[2] based on the reptation process alone, the viscosity in the entanglement regime is proportional to N^3 rather than $N^{3.4}$ as observed[25] experimentally. Constraint release (CR) and contour length fluctuations (CLF) are considered as the additional relaxation processes which are responsible for the onset of the viscosity $N^{3.4}$ dependence. When introducing these processes into tube model theories, strict reptation is achieved at a reptational molecular weight M_r, much larger than M_c, in agreement with rheological observations.[24,42] Moreover, it has been proposed that the ratio M_c/M_e is influenced[24] by CLF and CR. A common belief, which however is not valid,[24,43] is that the ratio takes a universal value close to two. In fact, Fetters et al.[24] have shown that M_c/M_e depends on the packing length, and as the latter increases the ratio decreases and approaches unity when $p \sim 9-10$ Å. Extrapolation of experimental data[24] suggests that at this packing length, $M_e = M_c = M_r$, so that for chain lengths larger than M_e, the system follows strict reptation and the onset is associated with a scaling law of $\eta \propto M^3$. The equality of M_e, M_c, M_r has been attributed to the relative strength of CLF, which is suppressed[24,25,42] for a large packing length.

It would be interesting to examine M_c/M_e as determined here by statics. The transition from Rouse-type to strict reptation dynamics is driven by the $L_{pp}(x)$ crossover presented in the previous section. Thus, the asymptotic chain length estimation for the dynamical/rheological crossover of D_{CM}, τ, η, is $N_e(\infty)$, the prediction for the rod to RW transition of PP conformations. Therefore, since M_c is provided by the η crossover, our scaling scheme leads always to an M_c/M_e ratio of 1. This prediction is independent of the N-variation of C_N, ν, and of the packing length, (which both affect the crossover regime and M_e). Nevertheless, the estimated ratio is in agreement with the fact that CLF corrections have been suppressed in the analysis, and that the scaling scheme for the rod to RW transition of PPs leads directly to strict reptation, a dynamical transition which experimentally appears for very large packing lengths, where

M_c/M_e approaches one. At this stage, it is unclear whether (packing length dependent) CLF corrections could lead to a crossover involving a $N^{3.4}$ power law in viscosity, (which becomes N^3 for very long chains), and a packing length dependent ratio larger than one. Such a scheme would be of great importance, since M_c and M_e could be estimated from shortest paths and their fluctuations.

3.9. One Entanglement per Chain. In order to examine topologically when all chains have at least one entanglement, we define the average number of entanglements per chain, Z, as

$$Z = \frac{N}{N_e(N)} - 1 = \frac{x}{\widetilde{N}_e(x)} - 1 = \frac{{L_{pp}}^2(x)}{R^2(x)} - 1 \qquad (26)$$

so that in the rod regime of PPs, $Z = 0$. $x = N - 1$ denotes the number of chain bonds. With this definition, when $Z = 1$, we have always $N = 2N_e(N)$, or $x = 2\widetilde{N}_e(x)$. In our data, this happens when $15 < N < 20$. In addition, when $Z = 1$, $L_{pp} = 2^{1/2}2R$, and $d \simeq 071R$. Figure 6a presents $Z(x)$ in semilog coordinates. As previously, our data set was enhanced by adding data for $N = 3$, 4, and 5. Below $N = 6$, our system is in the rod regime, so that $N_e(N) = N$ and $Z = 0$. Additional data are shown with open squares. We see that Z becomes linear with N gradually, at long chain lengths.

The solid line denotes eq 26, where $L_{pp}(x)$ and $C_N(x)$ have been calculated as in Figure 5b. The intersection of the dashed-dot line (denoting $Z = 1$) with the solid line defines N_{Z1}, the chain length where the PP consists of at least two Kuhn segments, i.e., $L_{pp}(x) = 2d(x)$. At the intersection $x \simeq 16.5$ and thus $N = N_{Z1} \sim 17.5$ and $N_e(N) = 8.75$. The condition $Z = 1$ does not necessarily lead to the onset of entangled rheological behavior, and thus N_{Z1} does not correspond to M_c.

The dashed line in Figure 6a denotes the asymptote at $Z = 0$, and the dotted line denotes the asymptote at $x \rightarrow \infty$, where Z is linear with N. That is,

$$Z \rightarrow \frac{(l_{cg} - \delta_\infty)^2}{C_\infty l_{cg}^2} x - 1 = \frac{x}{N_e(\infty)} - 1 \qquad (27)$$

From eq 27, for $Z = 0$, the intersection of the asymptotes in Figure 6a, similarly to Figure 5b, is at $x = N_e(\infty) \simeq 12.6$. The intersection of line $Z = 1$ with the asymptote at $x \rightarrow \infty$ is, by construction, at $x = 2N_e(\infty) = 25.2$. In Figure 6b we show the crossover in a Z-plot, as it appears in log−log coordinates. The length scales estimated here for N_{Z1} can be compared with global dynamics length scales in part II.[3]

An interesting issue is that, if entanglements are binary slip-links,[13−18] then geometrically $Z \simeq 1$ cannot lead to a percolated network at the length scale of $N_e(N)$. Percolation would occur for a Z between one and two. Otherwise, all chains would be linked into separate pairs, without the presence of an underlying network generated by binary links. Thus, assuming that the onset of entangled dynamics presupposes a percolated network of links, the simple notion $M_c \simeq 2M_e$, (or $Z = 1$), leads naturally to a number of TCs or links per chain which is larger than the number of entanglements per chain, so that percolation can occur. This is meaningful since entanglements are mean field objects. For example, within our data, when $Z \simeq 1$, we find $N_{Z1}/N_{TC} \simeq 4.8$, and thus the number of TCs per chain $Z_{TC} \simeq 3.8$. Packing length ideas also suggest that an entanglement is associated "with enough different chains getting into the same room together".[24,25,42,44] Thus, from statics alone, while most TCs in our model involve two chains and they are binary, at the length scale of N_e our microscopic analysis suggests that an entanglement is not binary.

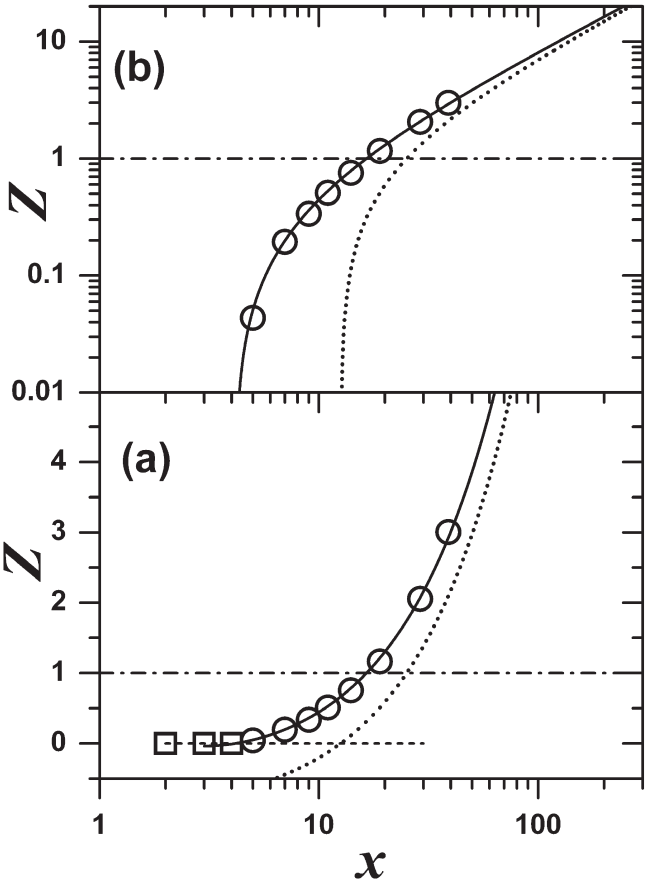

Figure 6. Number of entanglements per chain Z in semilog coordinates (a) and in log−log coordinates (b). Symbols as in previous figure. The dot-dashed line denotes $Z = 1$, the dashed line denotes the asymptote at $Z = 0$, the solid line denotes eq 26, and the dotted line denotes the asymptote at $x \rightarrow \infty$, given by eq 27. In the rod regime (where $Z = 0$), the dotted line in part b crosses the x-axis at $N_e(\infty)$, with an infinite slope. See text for an explanation.

3.10. Summary. It has been pointed[26,27,45] out, that there are two independent length scales in the entanglement problem. The Kuhn length, controlled by chain stiffness (e.g., the characteristic ratio), and the average distance between chain contours, controlled by density. In long chain polymer melts, the variation of these quantities between different species signifies changes in the degree of entanglement.[26] As discussed[27] by Colby et al., the presence of two independent length scales requires some conjecture about entanglements in order for scaling models to provide an answer (about the degree of entanglement between different species). Therefore, different models[27,43,46] make different predictions according to the chosen conjecture. The packing length model is based on a conjecture that leads to a very good correlation with polymer melt data. An overlooked point, related with the onset of entanglements, is that the stiffness and the density of any flexible polymer increase asymptotically as chain length increases.

For this reason, we have examined how the variation of these quantities, (which were treated here as varying length scales), leads to variations in the topology of a polymer melt and eventually to the onset of entanglements. We have shown that increasing chain length leads to increasing chain overlap, which is obvious, but at a rate which is smaller than in the asymptotic regime of long chains, where the rate is constant. This behavior is due to the asymptotic increase of stiffness and density with chain length, and leads to a crossover in the way chains interpenetrate each other.

Then, we have applied the CReTA algorithm[11] in order to reduce the melt systems to corresponding systems of primitive paths (PPs). This way, long chain systems are reduced to a network of interpenetrating shortest paths, generated by topological constraints (TCs). By probing the length scales related with the TCs we have shown that, as chain length increases, the underlying topology evolves toward a "homogeneous and invariant" regime. Homogeneous, in the sense that all chains are under the influence of TCs, and invariant in the sense that topological measures, such as the step length of PPs, do not change significantly with increasing chain length. Moreover, the contradiction related to the fact that TCs exist even for short chain systems (which are dynamically unentangled), a common finding in all recent static studies of PPs,[38−41] was explained qualitatively and quantitatively.

The onset of a long chain topology was then described in terms of a simple scaling model, inspired from an earlier work of Doi.[19] The model considers that the variation of PP length is due to a continuous transformation of PP conformations from thin rod-like objects (for short chains), to random walks (for long chains). The entanglement molecular weight is interpreted as the crossover length of this transformation.

Then we have associated the crossover in PP conformations with a crossover in dynamics and rheology. Our model does not consider contour length fluctuations (CLF) and it leads to a continuous transition of dynamics from Rouse-type to strict-reptation. It predicts an M_c/M_e ratio of one, admittedly small, but compatible with the suppression of CLF, and the fact that it is packing length independent.[24,25,42] In part II,[3] the static length scales deduced here are compared with dynamic length scales deduced from a Rouse mode analysis. We also compare the dynamical and rheological crossover deduced by the variation of PP length with the diffusion coefficient, the relaxation time of the end-to-end vector, and the viscosity of our systems. The agreement in the location of the crossover regime, by completely independent methods, i.e., statics and dynamics, is very good.

Acknowledgment. J.-M. Teuler is acknowledged for optimization and parallelization of the DPD code. The IDRIS supercomputing center (Orsay, France) is gratefully acknowledged for a generous allocation of computer time. The work of C.T. and D.N.T., in the context of this paper, is part of the Research Programme of the Dutch Polymer Institute (DPI), Eindhoven, The Netherlands, Project No. 650.

Appendix: Chain Slack Paradox

In a melt of RW-like chains, the chain slack per bond, δ, is smaller for a short, than a long chain system (see Figure 3d, Figure 5a). Correspondingly, the TC density is larger in the short chain regime than in the long chain asymptotic limit.

However, in the small-N regime, C_N and ν get smaller (see Figure 1), and then, packing length ideas suggest the opposite δ behavior. Namely, for entangled systems,[22,23,25] the more flexible the chains and the larger the distance between chain contours (thicker chains), the smaller the number of other chains penetrating the pervaded volume of a test chain. This leads to larger chain slack (larger M_e). The opposite behavior, revealed here for short systems, is due to chain ends again. CReTA constructs PPs as shortest paths by holding chain ends fixed[2,11] and shrinking simultaneously all chain contours. Thus, chain sections emanating from chain ends act as fixed obstacles to further shrinking of other chains. This way, a large chain end concentration leads to less chain slack per bond and more TCs. Another explanation is that short chains do not have enough length to generate unentangled loops which increase chain slack. We note that, by symmetry, since chain end sections act as fixed obstacles, the majority of TCs for a short chain system will be situated close to chain ends. Thus, in the context of tube models, our conjecture that the TCs for short chains (revealed by topological analysis) are short-lived and cannot promote reptation is meaningful.

References and Notes

(1) de Gennes, P. G. *Scaling concepts in polymer physics*; Cornell University Press: Ithaca, NY, 1979.
(2) Doi, M.; Edwards, S. F. *The theory of polymer dynamics*; Clarendon Press: Oxford, U.K., 1986.
(3) Lahmar, F.; Tzoumanekas, C.; Theodorou, D. N.; Rousseau, B. *Macromolecules* **2009**, DOI: 10.1021/ma9011329.
(4) Paul, W.; Smith, G. D. *Rep. Prog. Phys.* **2004**, *67*, 1117–1185.
(5) Padding, J. T.; Briels, W. J. *J. Chem. Phys.* **2001**, *115*, 2846–2859.
(6) Reith, D.; Meyer, H.; Müller-Plathe, F. *Comput. Phys. Commun.* **2002**, *148*, 299–313.
(7) Guerrault, X.; Rousseau, B.; Farago, J. *J. Chem. Phys.* **2004**, *121*, 6538–6546.
(8) Spenley, N. A. *Europhys. Lett.* **2000**, *49*, 534–540.
(9) Everaers, R.; Sukumaran, S. K.; Grest, G. S.; Svaneborg, C.; Sivasubramanian, A.; Kremer, K. *Science* **2004**, *303*, 823–826.
(10) Kröger, M. *Comput. Phys. Commun.* **2005**, *168*, 209–232.
(11) Tzoumanekas, C.; Theodorou, D. N. *Macromolecules* **2006**, *39*, 4592–4604.
(12) Tzoumanekas, C.; Theodorou, D. N. *Curr. Opin. Solid State Mater. Sci.* **2006**, *10*, 61–72.
(13) Shanbhag, S.; Park, S. J.; Zhou, Q.; Larson, R. G. *Mol. Phys.* **2007**, *105*, 249–260.
(14) Tasaki, H.; Takimoto, J. I. *Comput. Phys. Commun.* **2001**, *142*, 136–139.
(15) Shanbhag, S.; Larson, R. G. *Macromolecules* **2004**, *37*, 8160.
(16) Masubuchi, Y.; Ianniruberto, G.; Greco, F.; Marrucci, G. *Modell. Simul. Mater. Sci. Eng.* **2004**, *12*, S91–S100.
(17) Likhtman, A. E. *Macromolecules* **2005**, *38*, 6128–6139.
(18) Khaliullin, R. N.; Schieber, J. D. *Phys. Rev. Lett.* **2008**, *100*, 188302.
(19) Doi, M. *J. Phys. A: Math. Gen.* **1975**, *8*, 417–426.
(20) Mattice, W. L.; Suter, U. W. *Conformational theory of large molecules: the rotational isomeric state model in macromolecular systems*; John Wiley & Sons: New York, 1994.
(21) Karayiannis, N. C.; Giannousaki, A. E.; Mavrantzas, V. G.; Theodorou, D. N. *J. Chem. Phys.* **2002**, *117*, 5465–5479.
(22) Fetters, L. J.; Lohse, D. J.; Richter, D.; Witten, T. A.; Zirkel, A. *Macromolecules* **1994**, *27*, 4639–4647.
(23) Fetters, L. J.; Lohse, D. J.; Graessley, W. W. *J. Polym. Sci., Part B: Polym. Phys.* **1999**, *37*, 1023–1033.
(24) Fetters, L. J.; Lohse, D. J.; Milner, S. T.; Graessley, W. W. *Macromolecules* **1999**, *32*, 6847–6851.
(25) Fetters, L. J.; Lohse, D. J.; Colby, R. H. Chain dimensions and entanglement spacings. In *Physical properties of polymers handbook*, 2nd ed.; Mark, J. E., Ed.; Springer: Berlin, 2006; Chapter 25.
(26) Graessley, W. W.; Edwards, S. F. *Polymer* **1981**, *2*, 1329–1334.
(27) Colby, R. H.; Rubinstein, M.; Viovy, J. L. *Macromolecules* **1992**, *25*, 996–998.
(28) Rubinstein, M.; Colby, R. H. *Polymer physics*; Oxford University Press: Oxford, U.K., 2003.
(29) Padding, J. T.; Briels, W. J. *J. Chem. Phys.* **2001**, *114*, 8685–8693.
(30) Ferry, J. D. *Viscoelastics properties of polymers*; Wiley: New York, 1980.
(31) Kavassalis, T. A.; Noolandi, J. *Phys. Rev. Lett.* **1987**, *59*, 2674–2677.
(32) Kavassalis, T. A.; Noolandi, J. *Macromolecules* **1988**, *21*, 2869–2879.
(33) http://youtube.com/user/tzoumtube.
(34) Shanbhag, S.; Larson, R. G. *Macromolecules* **2006**, *39*, 2413–2417.
(35) Shanbhag, S.; Kröger, M. *Macromolecules* **2007**, *40*, 2897–2903.
(36) Larson, R. G.; Sridhar, T.; Leal, L. G.; McKinley, G. H.; Likhtman, A. E.; McLeish, T. C. B. *J. Rheol.* **2003**, *47*, 809–818.
(37) Lin, Y. H. *Macromolecules* **1987**, *20*, 3080–3083.
(38) Shanbhag, S.; Larson, R. G. *Phys. Rev. Lett.* **2005**, *94*, 76001.
(39) León, S.; van der Vegt, N.; Site, L. D.; Kremer, K. *Macromolecules* **2005**, *38*, 8078–8092.

(40) Foteinopoulou, K.; Karayiannis, N. C.; Mavrantzas, V. G.; Kröger, M. *Macromolecules* **2006**, *39*, 4207–4216.
(41) Foteinopoulou, K.; Karayiannis, N. C.; Laso, M.; Kröger, M. *J. Phys. Chem. B* **2009**, *113*, 442–455.
(42) McLeish, T. C. B. *Adv. Phys.* **2002**, *51*, 1379–1527.
(43) Wang, S. Q. *Macromolecules* **2007**, *40*, 8684–8694.
(44) Milner, S. T. *Macromolecules* **2005**, *38*, 4929–2939.
(45) Helfand, E. Photophysical and photochemical tools in polymer science. In *Photophysical and photochemical tools in polymer science*; Winnik, M. A., Ed.; Reidel: New York, 1986.
(46) Heynmans, N. *Macromolecules* **2000**, *33*, 4226–4234.